Transactions of Tianjin University (2023) 29:387–394
https://doi.org/10.1007/s12209-023-00365-y

RESEARCH ARTICLE

Ultrafast Carbonized Wood of Electrode-Scaled Aligned-Porous Structure for High-Performance Lithium Batteries

Shaojie Chen[1] · Lu Nie[1] · Hongsheng Shi[1] · Xiangchen Hu[1] · Zeyu Wang[1] · Xinshui Zhang[1] · Yuyao Zhang[1] · Qilin Hu[1] · Tianyi Gao[1] · Yi Yu[1,2] · Wei Liu[1,2,3]

Received: 19 April 2023 / Revised: 7 June 2023 / Accepted: 13 July 2023 / Published online: 1 September 2023

Abstract

The use of carbonized wood in various functional devices is attracting considerable attention due to its low cost, vertical channels, and high electrical conduction. However, the conventional carbonization method requires a long processing time and an inert atmosphere. Here, a microwave-assisted ultrafast carbonization technique was developed that carbonizes natural wood in seconds without the need for an inert atmosphere, and the obtained aligned-porous carbonized wood provided an excellent electrochemical performance as an anode material for lithium-ion batteries. This ultrafast carbonization technique simultaneously produced ZnO nanoparticles during the carbonization process that were uniformly distributed on the aligned-porous carbon. The hierarchical structure of carbonized wood functionalized with ZnO nanoparticles was used as a host for achieving high-performance lithium–sulfur batteries: the highly conductive carbonized wood framework with vertical channels provided good electron transport pathways, and the homogeneously dispersed ZnO nanoparticles effectively adsorbed lithium polysulfide and catalyzed its conversion reactions. In summary, a new method was developed to realize the ultrafast carbonization of biomass materials with decorated metal oxide nanoparticles.

Keywords Lithium–Sulfur battery · Shuttle effect · Lithium-ion battery · Biomass carbonization

Introduction

Wood is an abundant, sustainable, and biodegradable material with a natural hierarchical structure comprising well-oriented cellulose fibers and stomas that enable water, ion, and oxygen transportation. In recent years, there has been considerable interest in wood-derived materials and their use in a diverse range of applications, including bioengineering, flexible electronics, and clean energy [1–4], owing to their unique structural advantages, excellent mechanical performance, and versatile physicochemical properties. Carbonized wood (CW) is derived from natural wood at a low cost, and it retains the vertical channels and hierarchical porous structure while providing excellent electronic conduction; it is thus widely used as a catalyst carrier [5], gas adsorbent [6], and within various energy storage devices (supercapacitors and batteries) [7–11]. For example, Luo et al. [12] reported that mangrove-charcoal-derived carbon has a high discharge capacity of 335 mAh/g when used as an anodic material for lithium-ion batteries (LIBs).

Lithium–sulfur (Li–S) batteries are next-generation energy storage systems because they can be produced at a low cost, are environmentally friendly, and the S cathode has a high theoretical capacity (1675 mAh/g) [13–21]. However, the lithium polysulfide (LiPS) shuttle effect remains a critical obstacle to the practical application of Li–S batteries. In the charge and discharge process, soluble LiPS tends to shuttle between the cathode and anode, and it directly reacts with metallic Li in the anode, which results in a fast capacity decay, low Coulombic efficiency, and poor cycle life [22–24].

Numerous polar inorganic compounds (such as metal oxides [25–28], nitride [29, 30], carbide [31], and sulfide

✉ Wei Liu
liuwei1@shanghaitech.edu.cn

1 School of Physical Science and Technology, Shanghai Tech University, Shanghai 201210, China

2 Shanghai Key Laboratory of High-Resolution Electron Microscopy, Shanghai Tech University, Shanghai 201210, China

3 Key Laboratory of Advanced Energy Materials Chemistry (Ministry of Education), Nankai University, Tianjin 300071, China

[26, 32, 33],) have been used in Li–S batteries due to their high adsorption abilities and good catalytic conversion kinetics toward LiPS. In addition, various carbon materials are known to be good host materials for the S cathode, including carbon nanowires [34], carbon nanotubes [35], graphene [36, 37], and carbon frameworks [38]. Therefore, CW obtained from natural wood is a good potential host material for S. However, pyrolysis is a common carbonization method used to prepare CW [39–42], and a long processing time (> 6 h) and an inert atmosphere (N_2 or Ar) are required for pyrolysis, which makes this application problematic (Fig. 1a).

Herein, a microwave-assisted ultrafast carbonization technique (MAUCT) was developed to quickly carbonize wood in ~ 15 s (Fig. 1b). In this process, the wood is in direct contact with microwave-heated carbon, and no additional inert atmosphere is required. The obtained aligned-porous carbon provides a good electrochemical performance as an anode material for LIBs. Furthermore, due to the unique cellulose molecular chain structure, which is rich in oxygen-contained polar functional groups (for example, hydroxyl), zinc ions (Zn^{2+}) can effectively be coordinated [43]. The MAUCT simultaneously transforms $Zn(NO_3)_2$ into ZnO during the carbonization process, and a hierarchical carbonized wood structure decorated with ZnO nanoparticles (CW–ZnO) is obtained in one step. The highly conductive CW with vertical channels is an ideal free-standing and low-tortuosity host material for the S cathode, and the homogeneously dispersed ZnO nanoparticles effectively adsorb LiPS and catalyze its conversion reactions. As a result, Li–S cells using the CW–ZnO host provide good electrochemical performance.

Experimental Section

Preparation of Carbonized Wood (CW)

Natural wood was collected from eucalyptus trees. Wood was cut perpendicular to the growth direction, and small wood chips (10 mm × 10 mm × 1 mm) were obtained and dried at 200 °C for 10 h prior to carbonization. Using conventional pyrolysis method, the wood chips were transferred to a nitrogen-filled tube furnace and then heated at 1100 °C for 6 h. For microwave carbonization, the wood chips were placed in an alumina crucible, covered, buried with carbon black (CB, MTI corporation), and then transferred to a household microwave oven (Midea, M1-230E) to heat for 15 s.

Preparation of CW–ZnO

Natural wood was firstly cut and then immersed in 1 mol/L $Zn(NO_3)_2$ (Adamas-beta®) solution in vacuum for 48 h. After drying, the wood chips were microwave carbonized for 15 s to obtain the CW–ZnO product.

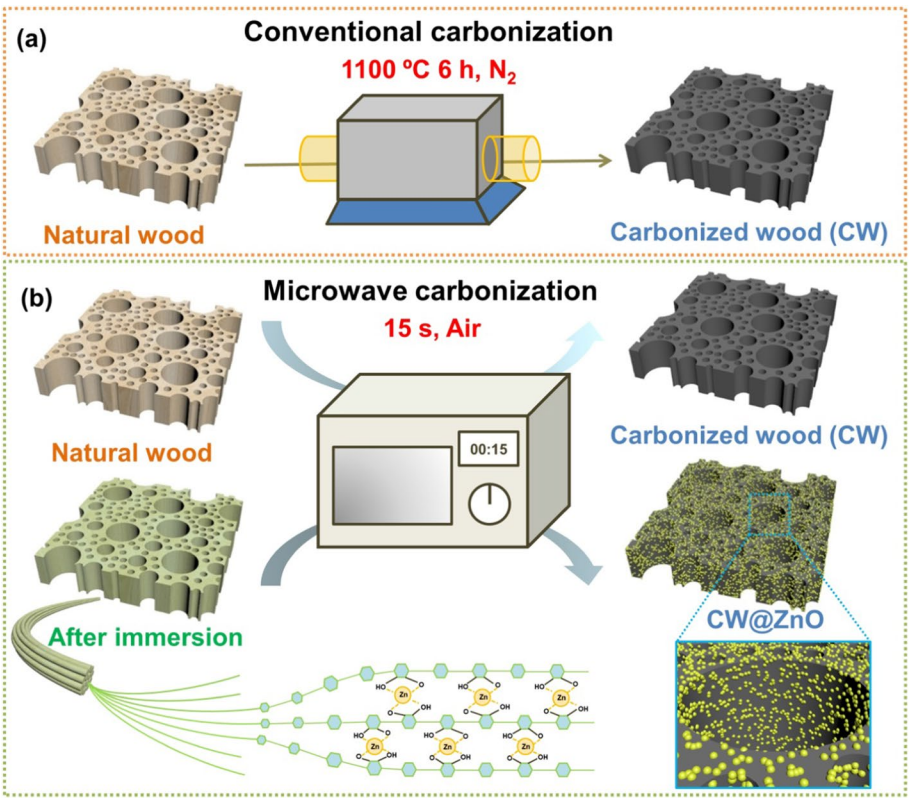

Fig. 1 Schematic of the two different carbonization methods. **a** A long processing time and an inert atmosphere are required for conventional carbonization; **b** a short processing time and operation in air are realized for microwave carbonization

Preparation of S@CW–ZnO Composite Cathode

A S/carbon disulfide (CS_2, Energy Chemical) solution was prepared at a concentration of 0.05 g/mL. The CW–ZnO chips were placed on aluminum foil, and the S/CS_2 solution was added with a pipette. The mass loading of S was ~ 3 mg/cm^2. The S@CW–ZnO composite had an S content of ~ 50 wt%.

Characterizations

The crystal structure was characterized by X-ray powder diffraction (XRD) (Bruker D8 Advance) using a Cu Kα radiation source. Elemental analyses were conducted using an elemental analyzer (PerkinElmer Clarus 580). Raman tests were performed on a Renishaw inVia equipped with a 532 nm laser. The morphology was characterized using a scanning electron microscope (SEM) (JEOL JSM-7800F) and transmission electron microscopy (TEM) (JEM 2100). The elemental content of the prepared CW was determined using a Clarus 580 elemental analyzer.

Electrochemical Measurements

To investigate the CW as an anode material for LIBs, the CW (~ 3.5 mg/cm^2), lithium foil (Adamas-beta®), and 1 mol/L $LiPF_6$ in ethylene carbonate/dimethyl carbonate (1:1, v/v ratio) were assembled into a coin 2032-type cell as the working electrode, counter electrode, and electrolyte, respectively. To investigate the S@CW–ZnO as a composite cathode for Li–S batteries, the coin cells were assembled with S@CW–ZnO, lithium foil (Adamas-beta®), and 1 mol/L lithium bis(trifluoromethanesulfonyl)imide (LiTFSI) in 1,3-dioxolane /dimethoxymethane (1:1, v/v ratio) with 1 wt% $LiNO_3$ as the cathode, anode, and electrolyte, respectively. The negative/positive electrode capacity ratio (N/P ratio) was ~ 18 because thick Li foil was used, and the electrolyte-to-S ratio (E/S ratio) was 20 µL/mg. The galvanostatic charge/discharge tests were measured using a LAND instrument and Neware battery cycler at room temperature. A cyclic voltammetry (CV) test was conducted on an electrochemical station (Bio-logic).

DFT Calculations

The Vienna Ab initio Simulation Package (VASP) is a computer program developed by Hafner's group [44] from the University of Vienna that is designed to conduct an atomic scale simulation from first principles. Simulations in the VASP are based on the Kohn–Sham density functional theory (KS-DFT), in which the exchange correlation potential can be approximated using the Perdew–Burke–Ernzerhof generalized gradient approximation (PBE-GGA) [45] in VASP. The electronic wave function was described using the projector augmented wave method [46]. In all the structure relaxations and self-consistent-field calculations, the convergence criterion of norms of all forces was 0.01 eV/Å for ionic relaxation, and the cutoff energy for the plane-wave-basis set was 450 eV.

TEM determined the space group of ZnO as $P6_3mc$. The (100) surface of ZnO had optimal stability [47]; therefore, the binding energy between LiPS and the (100) surface of ZnO was calculated. For the ZnO (100) crystal plane, a vacuum layer of 15 Å was introduced. A $3\times3\times1$ Monkhorst–Pack k-point mesh was used for the Brillouin zone. The binding energy, E_b, was calculated through $E_b = E_{LiPS} + E_{ZnO} - E_{LiPS+ZnO}$, where E_{LiPS}, E_{ZnO}, and $E_{Li\ PS+ZnO}$ represent the total energy of their respective systems.

Results and Discussion

XRD was used to determine the phase structure of the CW samples synthesized by both conventional carbonization and microwave carbonization. As shown in Fig. 2a, both XRD patterns presented two broad diffraction peaks located at ~ 23° and ~ 44° ssigned to the (002) and (101) crystal planes of graphite carbon [39]. Raman spectroscopy was conducted to further study the bonding structure (Fig. 2b), and the peaks at ~ 1350 and 1580 cm^{-1} for both carbonization methods corresponded to the D and G bands, respectively. The D-/G-band intensity (I_D/I_G) ratios of the CW samples synthesized by conventional carbonization and microwave carbonization were 0.96 and 0.83, respectively. The lower I_D/I_G intensity ratio indicated a higher degree of graphitization, suggesting that the microwave carbonization method provided a comparatively superior carbonization effect [39, 48]. The higher carbonization degree was also evidenced by the elemental analysis results presented in Table S1, in which the microwave-carbonized CW showed a higher carbon content (96.15%) than the conventional carbonized CW (94.01%). In addition, compared with the conventional carbonized CW, the microwave-carbonized CW showed lower O/C atomic ratio, indicating increased stability [49]. Furthermore, the yield of the CW prepared by MAUCT was 26.21 wt%, and the surface area of the CW prepared by MAUCT was 1.48 m^2/g, as determined by the BET test, which was larger than that of the CW obtained by conventional pyrolysis (0.75 m^2/g). The carbon-based anode material with a large surface area offered a greater number of Li-ion storage sites. These results showed that the use of MAUCT was more beneficial for preparing electrode materials from biomass.

To fabricate the CW–ZnO composite structure, a slice of natural wood was immersed in $Zn(NO_3)_2$ solution for

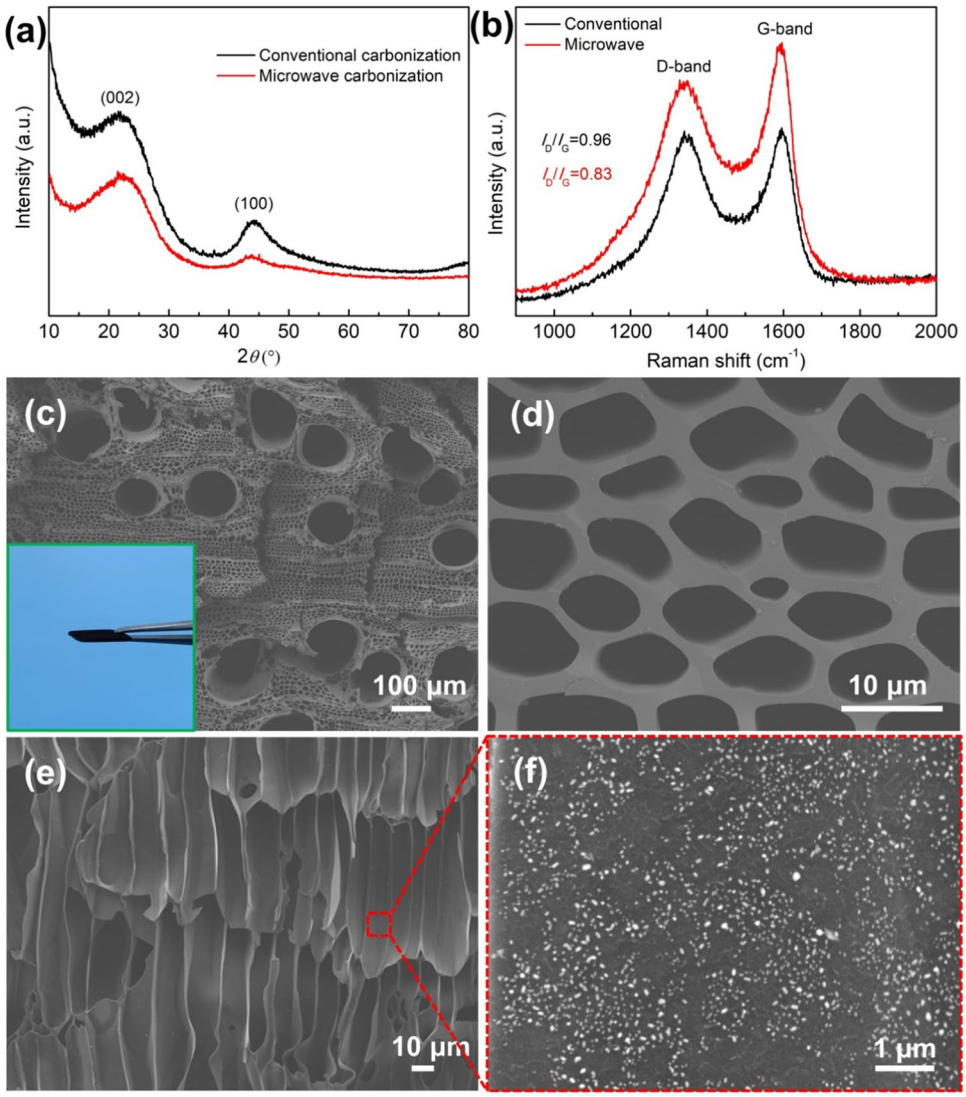

Fig. 2 Characterization of CW and CW–ZnO samples. **a** XRD patterns and **b** Raman spectra of the CW samples synthesized by conventional carbonization and microwave carbonization, respectively. **c** and **d** SEM images of the CW–ZnO sample. Inset: photograph of the CW–ZnO sample. **e** and **f** Cross-sectional SEM images of the CW–ZnO sample

two days in a vacuum. After drying, the wood was buried in carbon black powder for microwave carbonization. Owing to the excellent microwave-absorbing properties, carbon materials easily reach a high temperature above 1000 °C in seconds after absorbing microwaves, and this is known as carbothermal shock [50–52]. The above mechanism was adopted to swiftly carbonize natural wood and simultaneously transform $Zn(NO_3)_2$ into ZnO nanoparticles. The XRD results for CW–ZnO are shown in Fig. S1, where the peaks are seen to be consistent with those of the standard crystal structure of ZnO, thus indicating that ZnO can be formed using this method. The top-view SEM images of the CW–ZnO sample are displayed in Fig. 2c, d, where a porous structure with several large channels (100 μm) and numerous small channels (5–8 μm) is evident. Figure 2e shows a side-view SEM image of the CW–ZnO sample, in which the vertically aligned channels are evident. The high-magnitude SEM image (Fig. 2f) shows that ZnO nanoparticles are evenly distributed on the surface of the CW channels.

The TEM observations were conducted to further explore the microstructure of the CW–ZnO sample, and a thin slice of CW–ZnO was used for TEM characterization. As shown in Fig. 3a, numerous ZnO nanoparticles were homogeneously distributed on the surface of CW. The high-resolution TEM (HRTEM) image demonstrated that the particle size of the ZnO nanoparticle was ~ 20 nm, and the interplanar spacing was ~ 0.25 nm, corresponding to the (1 1 1) plane of ZnO. Furthermore, the Fourier transform pattern also evidenced the existence of the ZnO crystal structure (Fig. 3c), and energy-dispersive X-ray spectroscopy (EDS) mapping further proved the microstructure (Fig. 3d–f).

The CW material obtained by MAUCT without loading ZnO was first investigated as an anode for LIBs, and the charge–discharge curves at various current densities are presented in Fig. 4a, where the CW anode is seen to

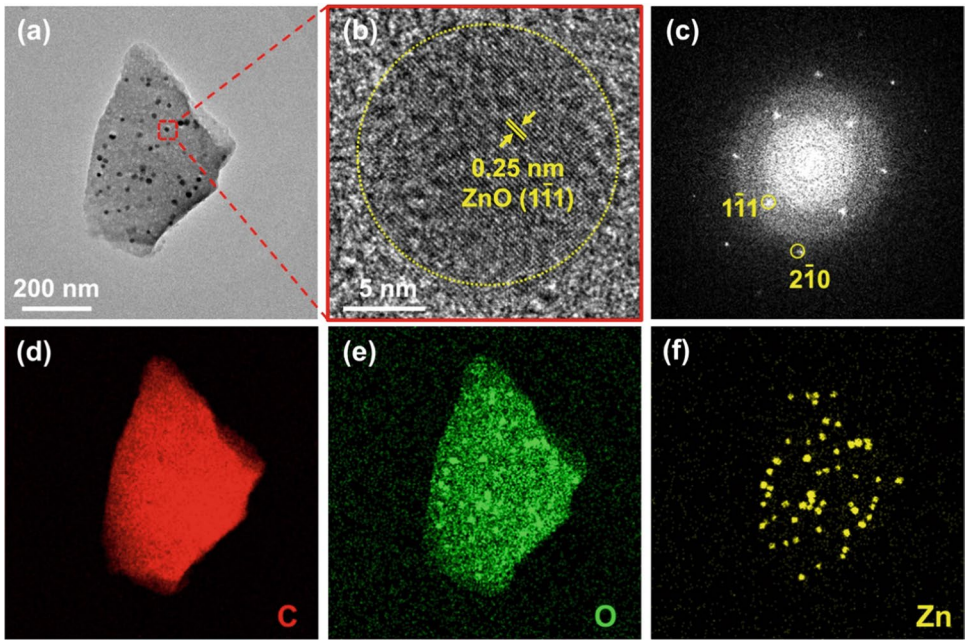

Fig. 3 TEM characterization of the CW–ZnO sample. **a** TEM image of the CW–ZnO sample. **b** HRTEM image and **c** Fourier transform pattern taken from the region within the red rectangle in **a**. **d–f** Corresponding EDS mapping images

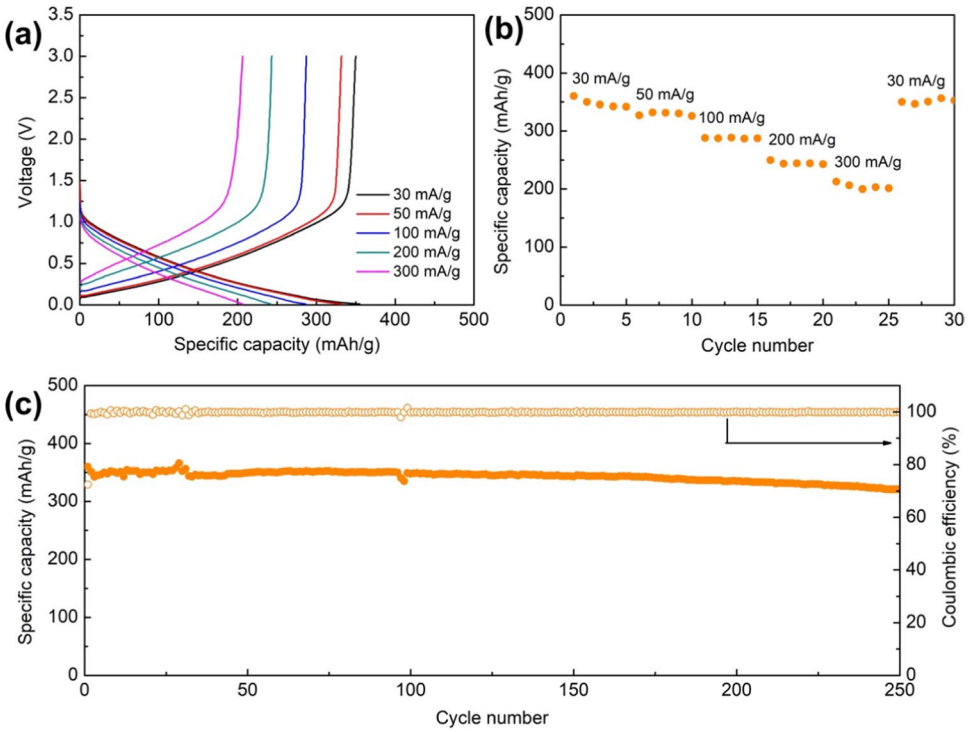

Fig. 4 Electrochemical performances of the CW as an anode material for LIBs. **a** Charge–discharge curves of the CW anode under various current densities. **b** Rate capability of the CW anode from 30 to 300 mA/g. **c** Long-term cycling performance and corresponding Coulombic efficiency

have achieved a high specific capacity of 350 mAh/g at 30 mA/g. As shown in Fig. 4b, even at a high current density of 300 mA/g, a satisfying capacity of ~ 210 mAh/g was maintained; this implied a good rate performance that was mainly contributed to the vertical channels and excellent electrical conductivity. Furthermore, when the current density reverted to 30 mA/g, the original capacity was recovered. The long-term cycling performance of the CW anode is shown in Fig. 4c, where the CW anode is shown to have achieved a long cycle life of over 250 cycles at 30 mA/g. As shown in Fig. S2, the porous structure of the CW anode was maintained after long-term cycling, indicating that the structural stability of the CW anode was good. Furthermore, high Coulombic efficiencies (> 99%) were realized after the first cycle, indicating good reversibility of Li-ion insertion and extraction.

The CW–ZnO hierarchical structure was used as a host material for S, and the electrochemical performances of the S@CW–ZnO cathode were studied. The results of the CV test at a scan rate of 0.1 mV/s are shown in Fig. 5a, where the reduction peaks at 2.3 V and 2.0 V correspond to the stepwise reduction of S to soluble LiPS and final insoluble Li_2S, respectively [28, 38], and the oxidation peaks at 2.4 V are associated with the reverse reaction. The charge–discharge curves at different cycles are shown in Fig. 5b. The S@CW–ZnO cathode achieved a high initial specific capacity of 1273 mAh/g at a C-rate of 0.1, but it also maintained a capacity of 480 mAh/g at a high C-rate of 2 C, suggesting that it provided a good rate performance (Fig. 5c). The S@CW–ZnO cathode also showed good long-term cycling stability, realizing a long cycle life of over 250 cycles (Fig. 5d). It also showed a lower initial

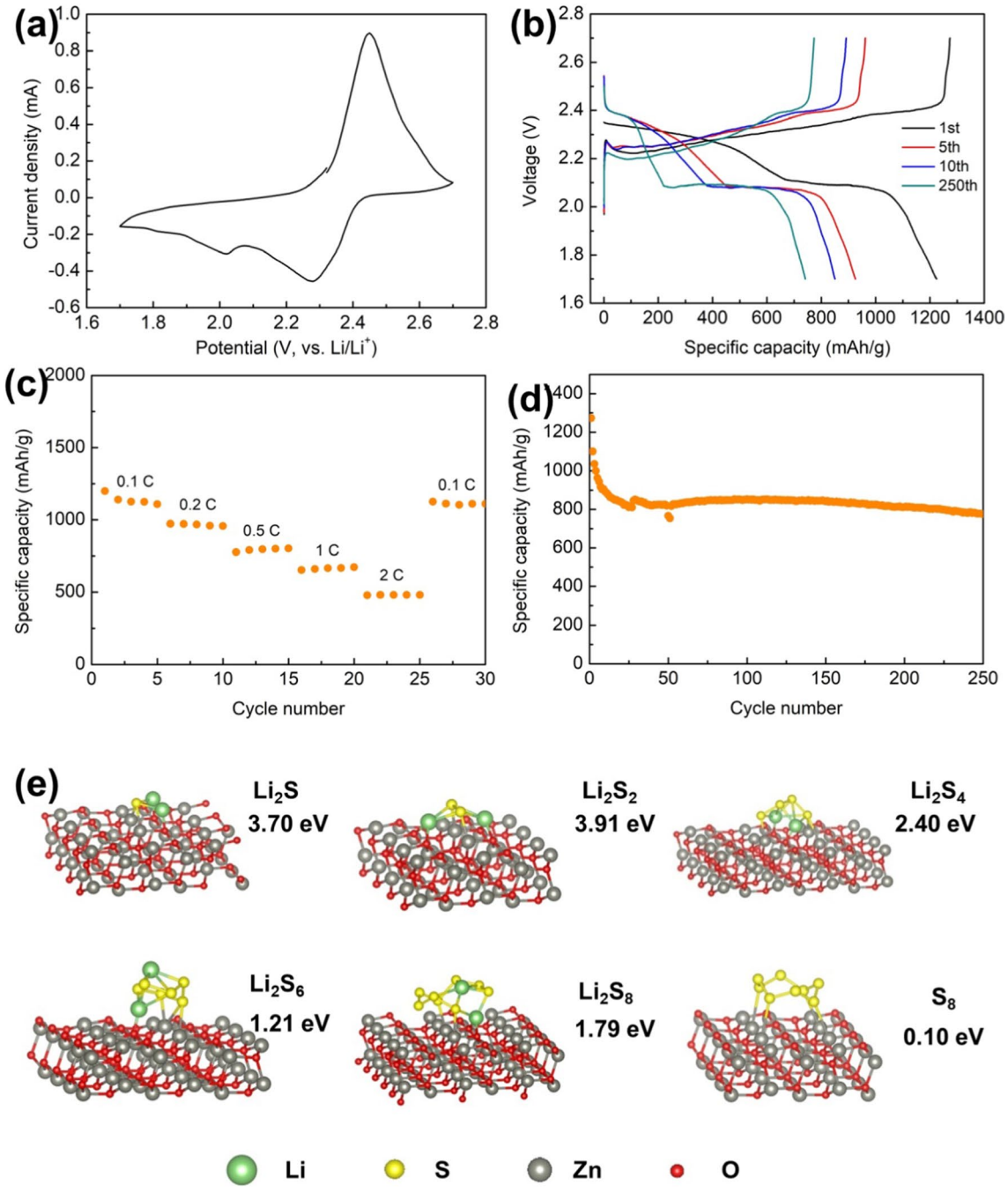

Fig. 5 Electrochemcial performance of the S@CW–ZnO composite cathode. **a** CV curve of the S@CW–ZnO composite cathode at 0.1 mV/s. **b** Charge–discharge profiles under different cycles. **c** Rate performance from 0.1 C to 2 C. **d** Cycling performance at 0.1 C. **e** Optimized chemisorption configurations of ZnO for binding LiPSs and S_8

specific capacity of 1160 mAh/g at a C-rate of 0.1, as shown in Fig. S3, and the specific capacity decreased severely after 250 cycles. The excellent electrochemical performances of the S@CW–ZnO cathode were mainly attributed to the hierarchical structure of the CW–ZnO host material. The CW skeleton with vertical channels decreased the diffusion paths of electrons and ions and accommodated the volume change of S during charging and discharging.

The functionalized ZnO nanoparticles also effectively adsorbed LiPS and catalyzed its redox kinetics. DFT calculations were employed to demonstrate the strong chemical interactions between ZnO and LiPS and S_8 (Fig. 5e). In the optimized chemisorption configurations, the S atom in LiPS preferred to bind with the Zn atoms, while the Li atom tended to bind with the O atoms. Furthermore, the ZnO showed high adsorption energy for the LiPSs and provided strong interactions to confine the LiPSs and enhance the conversion electrochemistry.

Conclusion

In summary, a MAUCT was developed that realizes the ultrafast synthesis of CW functionalized with metal oxide nanoparticles. Compared with the conventional pyrolysis method, the processing time was considerably reduced from an hour-level process to one that took seconds, and the need for an inert atmosphere was avoided. The CW obtained from MAUCT achieved a high specific capacity and a good rate capability, indicating its promising use as an anode material for LIBs. In addition, after immersing in $Zn(NO_3)_2$ solution, the ultrafast synthesis of CW decorated with a ZnO nanoparticle (CW–ZnO) hierarchical structure was obtained using MAUCT, and this provided a good electrochemical performance as a host material for Li–S batteries.

Supplementary Information The online version contains supplementary material available at https://doi.org/10.1007/s12209-023-00365-y.

Acknowledgements Shaojie Chen and Lu Nie contributed equally to this work. This work was partially supported by the National Natural Science Foundation of China (No. 52222311) and the Shanghai Rising-Star Program (20QA1406600). We also acknowledge CħEM, SPST of Shanghai Tech University (#EM02161943), Shanghai Science and Technology Plan (21DZ2260400) and Double First-Class Initiative Fund of Shanghai Tech University for supporting.

Declarations

Conflict of interest The authors declare that they have no conflict of interest.

References

1. Zhu HL, Luo W, Ciesielski PN et al (2016) Wood-derived materials for green electronics, biological devices, and energy applications. Chem Rev 116(16):9305–9374
2. Shan XF, Wu J, Zhang XT et al (2021) Wood for application in electrochemical energy storage devices. Cell Rep Phys Sci 2(12):100654
3. Jiang TY, Zhang YL, Olayiwola S et al (2022) Biomass-derived porous carbons support in phase change materials for building energy efficiency: a review. Mater Today Energy 23:100905
4. Qin GY, Huang XX, Yan X et al (2022) Carbonized wood with ordered channels decorated by $NiCo_2O_4$ for lightweight and high-performance microwave absorber. J Adv Ceram 11(1):105–119
5. Gan WT, Wu LP, Wang YX et al (2021) Carbonized wood decorated with cobalt-nickel binary nanoparticles as a low-cost and efficient electrode for water splitting. Adv Funct Mater 31(29):2010951
6. Yamashita R, Saito Y, Sakuragawa S (2009) Molecular sieving behavior of carbonized wood: selective adsorption of toluene from a gas mixture containing α-pinene. J Wood Sci 55(6):446–452
7. Huang JL, Zhao BT, Liu T et al (2019) Wood-derived materials for advanced electrochemical energy storage devices. Adv Funct Mater 29(31):1902255
8. Wu W, Wang X, Deng YY et al (2020) in situ synthesis of polyaniline/carbon nanotube composites in a carbonized wood scaffold for high performance supercapacitors. Nanoscale 12(34):17738–17745
9. Xin FE, Jia YF, Sun JE et al (2018) Enhancing the capacitive performance of carbonized wood by growing FeOOH nanosheets and poly(3, 4-ethylenedioxythiophene) coating. ACS Appl Mater Interfaces 10(38):32192–32200
10. Zhang WJ, Li M, Zhong L et al (2022) A family of MOFs@wood-derived hierarchical porous composites as freestanding thick electrodes of solid supercapacitors with enhanced areal capacitances and energy densities. Mater Today Energy 24:100951
11. Muruganantham R, Hsieh TH, Lin CH et al (2019) Bio-oil derived hierarchical porous hard carbon from rubber wood sawdust via a template fabrication process as highly stable anode for sodium-ion batteries. Mater Today Energy 14:100346
12. Liu T, Luo RY, Qiao WM et al (2010) Microstructure of carbon derived from mangrove charcoal and its application in Li-ion batteries. Electrochim Acta 55(5):1696–1700
13. Seh ZW, Sun YM, Zhang QF et al (2016) Designing high-energy lithium–sulfur batteries. Chem Soc Rev 45(20):5605–5634
14. Fu KK, Gong YH, Hitz GT et al (2017) Three-dimensional bilayer garnet solid electrolyte based high energy density lithium metal–sulfur batteries. Energy Environ Sci 10(7):1568–1575
15. Pang QA, Shyamsunder A, Narayanan B et al (2018) Tuning the electrolyte network structure to invoke quasi-solid state sulfur conversion and suppress lithium dendrite formation in Li–S batteries. Nat Energy 3(9):783–791
16. Pai R, Natu V, Sokol M et al (2021) Tuning functional two-dimensional MXene nanosheets to enable efficient sulfur utilization in lithium-sulfur batteries. Cell Rep Phys Sci 2(7):100480

17. Fan XY, Liu B, Liu J et al (2020) Battery technologies for grid-level large-scale electrical energy storage. Trans Tianjin Univ 26(2):92–103
18. Ji XY, Zhang YR, Cao MX et al (2022) Advanced inorganic/polymer hybrid electrolytes for all-solid-state lithium batteries. J Adv Ceram 11(6):835–861
19. Zhang C, Hu XC, Nie ZW et al (2022) High-performance Ta-doped $Li_7La_3Zr_2O_{12}$ garnet oxides with AlN additive. J Adv Ceram 11(10):1530–1541
20. Chen SJ, Zhang JX, Nie L et al (2021) All-solid-state batteries with a limited lithium metal anode at room temperature using a garnet-based electrolyte. Adv Mater 33(1):2002325
21. Nie L, Chen SJ, Zhang C et al (2022) Integration of a low-tortuous electrode and an in-situ-polymerized electrolyte for all-solid-state lithium-metal batteries. Cell Rep Phys Sci 3(4):100851
22. Bai SY, Liu XZ, Zhu K et al (2016) Metal–organic framework-based separator for lithium–sulfur batteries. Nat Energy 1(7):16094
23. Nanda S, Asl HY, Bhargav A et al (2022) Thiometallate-mediated polysulfide chemistry and lithium stabilization for stable anode-free lithium-sulfur batteries. Cell Rep Phys Sci 3(4):100808
24. Li W, Wang S, Fan Z et al (2021) Functionalized bacterial cellulose as a separator to address polysulfides shuttling in lithium–sulfur batteries. Mater Today Energy 21:100813
25. Tao XY, Wang JG, Liu C et al (2016) Balancing surface adsorption and diffusion of lithium-polysulfides on nonconductive oxides for lithium–sulfur battery design. Nat Commun 7:11203
26. Liu X, Huang JQ, Zhang Q et al (2017) Nanostructured metal oxides and sulfides for lithium–sulfur batteries. Adv Mater 29(20):1601759
27. Li W, Hicks-Garner J, Wang J et al (2014) V_2O_5 polysulfide anion barrier for long-lived Li–S batteries. Chem Mater 26(11):3403–3410
28. Chen SJ, Zhang JX, Wang ZY et al (2021) Electrocatalytic $NiCo_2O_4$ nanofiber arrays on carbon cloth for flexible and high-loading lithium–sulfur batteries. Nano Lett 21(12):5285–5292
29. Zhou WD, Xiao XC, Cai M et al (2014) Polydopamine-coated, nitrogen-doped, hollow carbon–sulfur double-layered core–shell structure for improving lithium–sulfur batteries. Nano Lett 14(9):5250–5256
30. Zhou X, Yang JL, Li NR et al (2022) Highly catalytic porous MoN nanosheets anchored carbon microtubes interlayer for lithium-sulfur batteries. Mater Today Energy 24:100941
31. Peng HJ, Zhang G, Chen X et al (2016) Frontispiece: enhanced electrochemical kinetics on conductive polar mediators for lithium–sulfur batteries. Angew Chem Int Ed 55(42):12990–12995
32. Liang XA, Hart C, Pang QA et al (2015) A highly efficient polysulfide mediator for lithium–sulfur batteries. Nat Commun 6:5682
33. Li S, Xu P, Aslam MK et al (2020) Propelling polysulfide conversion for high-loading lithium–sulfur batteries through highly sulfiphilic $NiCo_2S_4$ nanotubes. Energy Storage Mater 27:51–60
34. Chung SH, Manthiram A (2018) Designing lithium-sulfur cells with practically necessary parameters. Joule 2(4):710–724
35. Zheng GY, Yang YA, Cha JJ et al (2011) Hollow carbon nanofiber-encapsulated sulfur cathodes for high specific capacity rechargeable lithium batteries. Nano Lett 11(10):4462–4467
36. Ji LW, Rao MM, Zheng HM et al (2011) Graphene oxide as a sulfur immobilizer in high performance lithium/sulfur cells. J Am Chem Soc 133(46):18522–18525
37. Wang HL, Yang YA, Liang YY et al (2011) Graphene-wrapped sulfur particles as a rechargeable lithium–sulfur battery cathode material with high capacity and cycling stability. Nano Lett 11(7):2644–2647
38. Wang NN, Zhang XA, Ju ZY et al (2021) Thickness-independent scalable high-performance Li–S batteries with high areal sulfur loading via electron-enriched carbon framework. Nat Commun 12:4519
39. Gu YE, Ye MX, Wang YC et al (2020) Lignosulfonate functionalized g-C_3N_4/carbonized wood sponge for highly efficient heavy metal ion scavenging. J Mater Chem A 8(25):12687–12698
40. Huang JX, Wan HJ, Li MA et al (2021) In-situ growth of MAX phase coatings on carbonised wood and their terahertz shielding properties. J Adv Ceram 10(6):1291–1298
41. Luo C, Zhu HL, Luo W et al (2017) Atomic-layer-deposition functionalized carbonized mesoporous wood fiber for high sulfur loading lithium sulfur batteries. ACS Appl Mater Interfaces 9(17):14801–14807
42. Li MX, Cheng LF, Ye F et al (2021) Formation of nanocrystalline graphite in polymer-derived SiCN by polymer infiltration and pyrolysis at a low temperature. J Adv Ceram 10(6):1256–1272
43. Yang CP, Wu QS, Xie WQ et al (2021) Copper-coordinated cellulose ion conductors for solid-state batteries. Nature 598(7882):590–596
44. Kresse G, Furthmüller J (1996) Efficient iterative schemes forab initiottotal-energy calculations using a plane-wave basis set. Phys Rev B 54(16):11169–11186
45. Perdew JP, Burke K, Ernzerhof M (1996) Generalized gradient approximation made simple. Phys Rev Lett 77(18):3865–3868
46. Blöchl PE, Jepsen O, Andersen OK (1994) Improved tetrahedron method for brillouin-zone integrations. Phys Rev B 49(23):16223–16233
47. Meyer B, Marx D (2003) Density-functional study of the structure and stability of ZnO surfaces. Phys Rev B 67(3):035403
48. Yu RH, Wen X, Liu J et al (2021) A green and high-yield route to recycle waste masks into CNTs/Ni hybrids via catalytic carbonization and their application for superior microwave absorption. Appl Catal B 298:120544
49. Gabhi R, Basile L, Kirk DW et al (2020) Electrical conductivity of wood biochar monoliths and its dependence on pyrolysis temperature. Biochar 2(3):369–378
50. Xu SM, Zhong G, Chen CJ et al (2019) Uniform, scalable, high-temperature microwave shock for nanoparticle synthesis through defect engineering. Matter 1(3):759–769
51. Zhong G, Xu SM, Chen CJ et al (2019) Synthesis of metal oxide nanoparticles by rapid, high-temperature 3D microwave heating. Adv Funct Mater 29(48):1904282
52. Chen SJ, Nie L, Hu XC et al (2022) Ultrafast sintering for ceramic-based all-solid-state lithium-metal batteries. Adv Mater 34(33):2200430

Wei Liu received her BS degree in materials physics from Beijing Normal University in 2008 and her PhD degree in materials science and engineering from Tsinghua University in 2013. She visited the University of Tokyo during 2010–2011. From 2013 to 2017, she was a postdoctoral scholar at Stanford University. She joined ShanghaiTech University as an assistant professor in 2017. Her research interests cover the area of solid-state ionics and nanotechnology, with a focus on the studies of lithium batteries.